

Non-uniform Sediment Transport around a Spur Dyke

Hao ZHANG*¹, Hajime NAKAGAWA² and Hideaki MIZUTANI³

¹Dr. of Eng., Assist. Prof., Disaster Prevention Research Institute, Kyoto University, Japan,
E-mail: zhang@uh31.dpri.kyoto-u.ac.jp

²Dr. of Eng., Prof., Disaster Prevention Research Institute, Kyoto University, Japan

³Hydro-soft Technology Institute, Co., Ltd, Osaka, Japan

Abstract

This paper describes a study on non-uniform sediment transport around a spur dyke with both experimental and numerical methods. A series of experiments were conducted in a laboratory flume with/without a spur dyke protruding to a movable bed consisting of uniform/non-uniform sediment. The bed variations in terms of both elevation and bed-materials composition are measured with advanced experimental facilities. A numerical model was developed based on an unstructured mesh to simulate the complex local flow and bed variations around the spur dyke. The flow velocity is simulated with a 3D k- ϵ turbulence model. A non-equilibrium sediment transport model was adopted considering both stochastic and deterministic nature of the movement of sediment particles. The simulation results are consistent with those of the experiments. Based on the research results, the effects of sediment mean size and size distribution on scour-deposition patterns and bed compositions around a spur dyke are discussed and characterized.

Keywords: non-uniform sediment, spur dyke, scour-deposition

1. Introduction

Local bed deformation around a spur dyke is a conventional research topic in the hydraulic engineering. From simple empirical predictions of the maximum scour depth to advanced numerical simulations of the local scour process, a lot of engineers and researchers have contributed to this problem. A review of those researches has been made by Zhang and Nakagawa (2008a). However, the development of human society and the changing of public awareness always pose new requirements and challenges for scientific researches. Existing knowledge is likely to soon becoming insufficient nowadays. With the significant increasing of environmental concerns, investigation on the

processes or parameters having implications of the quality and structure of riverine habitats, is receiving more and more attention in the hydraulic engineering.

As one of the most typical human-introduced measures in the hydraulic engineering, a spur dyke has been widely placed in natural rivers. In general, spur dykes were designed to protect channel banks and to improve navigation conditions. But the positive impacts on river environment have been confirmed in experiments and actual rivers. As a result, investigation on the environmental implications of spur dykes is of great interest recently. It is well known that natural riverbeds are generally characterized by non-uniform sediment, consisting of a wide spectrum of particle sizes.

Investigation on the transport of the mixture of those particles is of practical value to estimate and to characterize the responses of channel morphologies as well as riverine habitats. Unfortunately, researches taking into account non-uniform sediment transport are still very few, in particular in case of the involvement of spur dykes. During the bed evolution process, the main difference between a non-uniform bed and a uniform bed is the selective transport of sediment particles, known as sediment sorting. The direct result of sediment sorting is that the bed surface is in shortage of fine particles and an armor layer forms there. The fine particles may deposit in some area or be transported to the downstream of the river. The armor layer may become a shelter for fine particles beneath it, preventing the bed from degradation or be destroyed in some event. The non-uniformity of sediment particles exerts great impacts on the local scour process and bed composition in the proximity of the spur dyke. However, the problem has never been clarified up to date.

In this paper, the changes of the bed level and the bed composition around an impermeable spur dyke are investigated with experimental and numerical methods under non-uniform sediment transport conditions. Additional to conventional parameters such as the maximum local scour depth and scour hole area, special attention is paid to the spatial distribution of sediment sizes in the

neighborhood of the spur dyke.

2. Laboratory Experiments

2.1 Experiment setup

A series of experiments have been carried out in a straight tilting flume at the Ujigawa Open Laboratory, Kyoto University. The flume is 8m-long, 40cm-wide and 40cm-deep, with a 1.5m-long inlet tank upstream (Fig.1). A working area locates 4m downstream from the inlet tank. It is 1.7m long and is covered with 20cm-thick sediment: silica sand. The upstream and downstream parts of the working area are fixed with 20cm-thick wooden boards. A 50cm-long sediment trap is set at the end of the flume, followed by a tailgate. Experiments are carried out under two scenarios: with no hydraulic structure in the flume or with an impermeable spur dyke attached to the flume. In the latter scenario, the spur dyke is 1cm-thick and is perpendicular to the right side of the flume with a protruding length of 10cm.

The hydraulic conditions and specification of the experimental cases are shown in Tab.1 and Tab.2. Totally, 10 experiments have been conducted under the same flow conditions. From Case1 to Case6, relatively uniform sediment bed is prepared in the working area. Case7 and Case8 deal with gap-graded sediment bed consisting of particles with two obviously distinguished size fractions. In Case9 and

Unit: cm

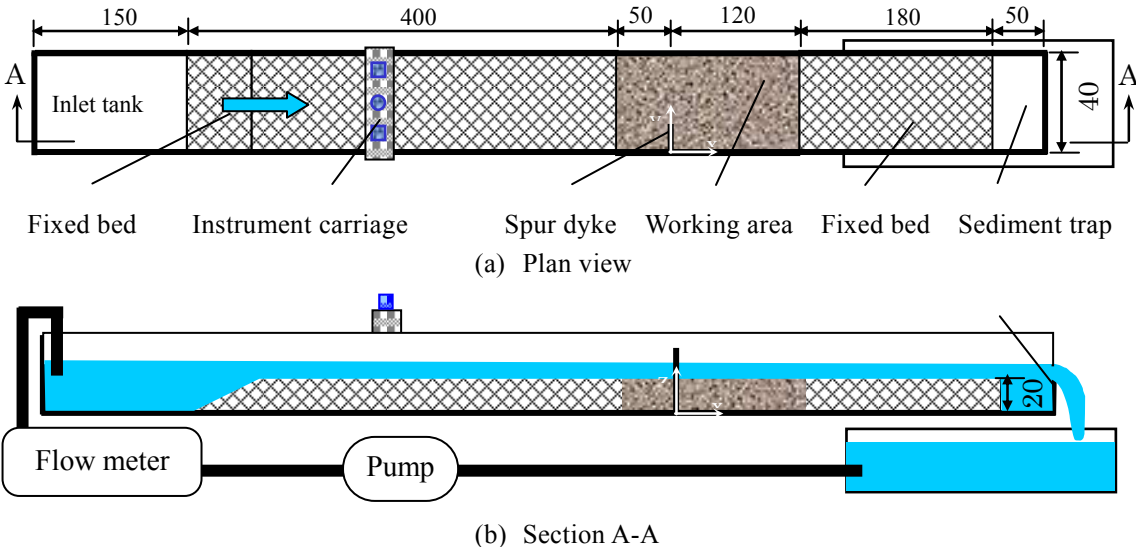


Fig.1 Experimental flume and setup

Case10, the distribution curve of sediment sizes is relatively smooth and the sediment bed is considered as well graded.

Table1 Experiment cases

Case	Spur	D (mm)	σ_g	u_* / u_{*c}
Case1	No	1.03	1.229	0.832
Case2	Yes			
Case3	No	1.70	1.183	0.622
Case4	Yes			
Case5	No	0.31	1.356	1.177
Case6	Yes			
Case7	No	1.00	2.323	0.846
Case8	Yes			
Case9	No	0.86	2.080	0.909
Case10	Yes			

Table2 Hydraulic conditions

Flow discharge (l/s)	5.7
Channel slope	1/1000
Channel width (cm)	40
Flow depth (cm)	5.0
Flow velocity (cm/s)	29.0
Friction velocity (cm/s)	1.98
Sediment density (g/cm ³)	2.65
Spur length (cm)	10.0
Spur thickness (cm)	1.0
Reynolds number	14, 250
Froude number	0.41

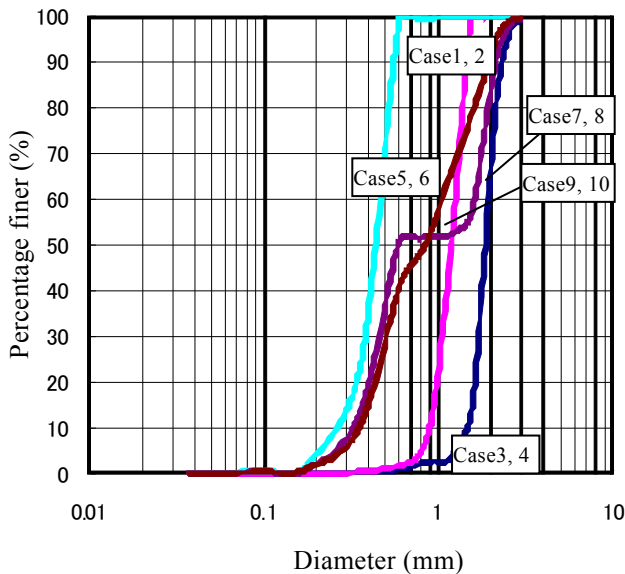


Fig. 2 Size distribution of sediment particles

The mean diameters of sediment particles either in Case 7, 8 or in Case9, 10 are very close to those in Case1, 2. Furthermore, in case of uniformly

graded bed, sediment particles with much larger diameters (i.e. Case3, 4) or much smaller diameters (i.e. Case5, 6) than those of Case1, 2 have been adopted. Sediment size distribution at the initial bed in each case is shown in Fig.2.

2.2 Experiment procedure

Sediment is filled in the working area to make the movable bed. Before each experimental run, the sediment bed surface is leveled with a scraper blade mounted on a carriage riding on the rails over the model channel banks. After that, the flume is slowly filled with water. When the desired water depth is achieved, the pump is started with the designated discharge and experiment starts. In cases with a spur dyke, the spur dyke is non-submerged. Moreover, the approach flow velocity is less than the critical flow velocity for the sediment entrainment except in Case5, 6. Channel beds in Case1 and Case3 are unchanged under the current flow condition. Hence the bed variations are not measured. Basically, each experiment is carried out for 3hours. For non-uniform bed cases without any hydraulic structure (i.e. Case7, 9), the bed sorting process seems very slow. Experiments are continued for 6.5hours. After the completion of each experiment, the flume is drained out and the bed configuration is measured with a high-resolution laser displacement meter (Model LK-500, Keyence, co., Ltd.). After that, sediment samples are taken from the bed surface (about 2.8mm thick) at several representative locations. The size distributions of the samples are analyzed with a nested column of sieves, together with a high-resolution balance scale (UW220H, Shimazu, co., Ltd.).

3. Numerical Model and Simulations

A 3D numerical model is developed to simulate the complex flow, sediment transport and bed variation in the neighborhood of the spur dyke. The model consists of a hydrodynamic module, a sediment transport module and a bed variation module. The approach employed in this model may be classified as an Euler-Lagrange coupling type, in which the flow and sediment are treated in quite different ways. The details of the three modules are presented hereafter.

3.1 Numerical model details

(1) Hydrodynamic module

In order to simulate complex turbulent flow phenomena in complex geometries, Zhang (2005) has developed a 3D numerical model based on the unsteady RANS (Reynolds-averaged Navier-Stokes equations) with the widely-used k - ε equations for the turbulence closure. The governing equations written in the tensor form with the convention of Einstein summation are as follows.

$$\frac{\partial u_j}{\partial x_j} = 0 \quad (1)$$

$$\frac{\partial u_i}{\partial t} + u_j \frac{\partial u_i}{\partial x_j} = f_i - \frac{1}{\rho} \frac{\partial p}{\partial x_i} + \nu \frac{\partial^2 u_i}{\partial x_j \partial x_j} + \frac{1}{\rho} \tau_{ij} \quad (2)$$

$$\frac{\partial k}{\partial t} + u_j \frac{\partial k}{\partial x_j} = \frac{\partial}{\partial x_j} \left[\left(\nu + \frac{\nu_t}{\sigma_k} \right) \frac{\partial k}{\partial x_j} \right] + G - \varepsilon \quad (3)$$

$$\frac{\partial \varepsilon}{\partial t} + u_j \frac{\partial \varepsilon}{\partial x_j} = \frac{\partial}{\partial x_j} \left[\left(\nu + \frac{\nu_t}{\sigma_\varepsilon} \right) \frac{\partial \varepsilon}{\partial x_j} \right] + (C_{1\varepsilon} G - C_{2\varepsilon} \varepsilon) \frac{\varepsilon}{k} \quad (4)$$

where u_i, u_j = velocity components; x_i, x_j = Cartesian coordinate components; ρ = the density of the fluid; f_i = body force components; p = the pressure field; ν = the molecular kinematic viscosity of the fluid; τ_{ij} = Reynolds stresses. Due to the existence of the Reynolds stress terms, equation system Eq. (1) and Eq. (2) is not closed. In a k - ε model, the Reynolds stresses are evaluated from the information of the mean flow after introducing a concept of eddy viscosity ν_t and constructing two transport equations, i.e. Eq. (3) and Eq. (4), for the turbulence kinetic energy k and its dissipation rate ε . Then the Reynolds stress terms are estimated from the following expression.

$$\tau_{ij} = -\overline{\rho u_i' u_j'} = 2\rho \nu_t S_{ij} - \frac{2}{3} \rho k \delta_{ij} \quad (5)$$

where

$$\nu_t = C_\mu \frac{k}{\varepsilon} \quad S_{ij} = \frac{1}{2} \left(\frac{\partial u_i}{\partial x_j} + \frac{\partial u_j}{\partial x_i} \right) \quad \delta_{ij} = \begin{cases} 1 & \text{if } i = j \\ 0 & \text{if } i \neq j \end{cases}$$

in which u_i', u_j' = the fluctuating velocity component in i, j direction, respectively; ν_t = the eddy viscosity; S_{ij} = the strain-rate tensor, δ_{ij} = the Kronecker delta and C_μ = coefficient, being usually set as a constant 0.09. In the transport equations for k and ε , G = the rate of turbulence production and is defined as

$$G = -\overline{u_i' u_j'} \frac{\partial u_i}{\partial x_j} \quad (6)$$

The model parameters in Eq. (3) and Eq. (4) generally take the following values for practical use.

$$\sigma_k = 1.0 \quad \sigma_\varepsilon = 1.3 \quad C_{1\varepsilon} = 1.44 \quad C_{2\varepsilon} = 1.92 \quad (7)$$

The governing PDEs (Partial differential equations) are integrated over a series of control volumes covering the study domain with an FVM (Finite volume method). The conserved equations are discretized on a collocated unstructured mesh. The power law scheme has been adopted during the spatial discretization. The surface fluxes are calculated from the Rhie-Chow momentum interpolation method in order to avoid the so-called checkerboard phenomenon. For the temporal integral, the second order implicit Crank-Nicolson scheme is employed. The widely used SIMPLE (Semi-implicit method for pressure-linked equations) procedure is included in the model for the coupling of the pressure and the velocity. The final algebraic equations resulted from the discretization process are solved with a preconditioned GMRES (Generalized minimal residual method) incorporated with an ILUTP (Incomplete LU factorization with threshold and pivoting) preconditioner. The detailed discretization and solution methods are referred to Zhang (2005).

(2) Sediment transport module

Modeling of the sediment transport process and its morphological consequences is a bottleneck of the application of numerical methods in the hydraulic engineering nowadays. It is mostly due to the shortage of a clear understanding and description, preferably in a mathematic form, of the associated physical process. This process is quite sophisticated. If only bedload is considered, the movement of a sediment particle may be divided into a three-stage process: be picked up from the bed, transport near the bed and deposit onto the bed. If these three stages could be quantified, the sediment movement and bed deformation were able to be simulated. It is known that for an individual particle, its movement must follow the basic mechanical laws. On the other hand, when a group

of sediment particles are concerned, the problem may turn into a stochastic problem in which the turbulence flows, the bed conditions and the interparticle collisions are all uncertain. In this paper, the problems related to the sediment pick-up and deposition are considered as stochastic problems and those related to the transport stage are treated in a deterministic way. In order to estimate the bed variation process, the following modeling procedure is proposed. Firstly, the amount of sediment of different sizes being picked up at any specified location is estimated. After that the trajectory of each sediment size fraction is sought. Then, the deposition amount of sediment particles along each trajectory is estimated. The deposition amount is interpolated to any specified computation point if necessary. By introducing an algorithm for bed sorting, the temporal bed variation in terms of both configuration and composition is obtained finally.

a) Sediment pick-up

Considering the effect of local bed slope, Nakagawa et al. (1986) has proposed the following expression to estimate the pick-up rate of sediment particles from a bed.

$$p_{s(k)} \sqrt{\frac{d_{(k)}}{(\sigma/\rho-1)g}} = F_0 G_* \tau_{*k} \left(1 - \frac{k_p \Phi \tau_{*ck}}{\tau_{*k}} \right)^{m_p} \quad (8)$$

in which

$$G_* = \frac{\cos \psi + k_L \mu_s}{1 + k_L \mu_s}$$

$$\tau_{*k} = \frac{u_*^2}{(\sigma/\rho-1)gd_{(k)}}$$

$$\Phi = \frac{\mu_s \cos \theta_b - \sin \theta_b \cos \alpha}{\cos \psi + k_L \mu_s} \frac{1 + k_L \mu_s}{\mu_s}$$

where $p_{s(k)}$ = pick-up rate for size fraction k ; $d_{(k)}$ = the diameter of size fraction k ; σ = the density of sediment; F_0 , k_p and m_p are constants (=0.03, 0.7 and 3, respectively) as suggested by Nakagawa et al. (1986); G_* = coefficient accounting for the direction deviation between near bed velocity and sediment movement direction; ψ = the angle between the near bed velocity and the sediment movement direction; τ_{*k} = the dimensionless shear stress for size fraction k ; u_* = the near-bed friction velocity; τ_{*ck} = the dimensionless critical shear stress for size fraction k ; Φ = coefficient accounting for local bed

slope; μ_s = the static friction factor (=0.7); k_L = the ratio of lift force to drag force (=0.85); θ_b = the local bed slope; α = the angle between the maximum local bed slope and sediment movement direction. In the computational domain, the volume of sediment being picked up from a mesh is then estimated from the following expression.

$$V_{p(k)} = \frac{A_3 d_{(k)}}{A_2} p_{s(k)} S_p P_{b(k)} \quad (9)$$

where $V_{p(k)}$ = sediment pick-up volume of size fraction k from a mesh; S_p = projected area of the computational mesh onto the horizontal plane; $p_{b(k)}$ = percentage of sediment of size fraction k in the bed surface; A_2 , A_3 = shape coefficients of sediment particles for 2D and 3D geometrical properties (= $\pi/4$ and $\pi/6$, respectively). Nagata et al. (2005) and Onda et al. (2007) employed this method for uniform sediment beds and verified its applicability. In this study, it is extended to non-uniform beds. It is noted that the availability of sediment particles of any size fraction in the bed surface layer has been considered in Eq. (9).

b) Trajectory of sediment movement

After being picked up, sediment particles will move near the bed and some of them may deposit onto the bed somewhere. The sediment movement velocity and information on the trajectory of the movement of sediment particles are of importance. Omitting the inter-particle collisions, the movement velocity \mathbf{u}_{sed} of a sediment particle is estimated from its moment equation. Defining two unit vectors paralleling to the local bed surface: \mathbf{p}_{b1} on xz -plane and \mathbf{p}_{b2} on yz -plane, the moment equation in \mathbf{p}_{bj} direction is written as below for a particle belonging to size fraction k .

$$\rho \left(\frac{\sigma}{\rho} + C_m \right) A_3 d_{(k)}^3 \frac{du_{sedj}}{dt} = D_{kj} + W_{kj} - F_{kj} \quad (j=1,2) \quad (10)$$

in which u_{sedj} = component of sediment movement velocity in j direction; C_m = coefficient of added mass; D_{kj} = component of drag force on a particle in j direction; W_{kj} = component of submerged weight of sediment particle in j direction; F_{kj} = component of friction force between sediment particle and the bed in j direction. The magnitude of the drag force, particle submerged weight and friction force are obtained as below

$$D_{(k)} = \frac{C_D \rho}{2} (u_{bj} - u_{sedj})^2 c_e A_2 d_{(k)}^2 \quad (11)$$

$$W_{(k)} = (\sigma - \rho) g A_3 d_{(k)}^3 \quad (12)$$

$$F_{(k)} = \mu_k \left(W_{(k)} \frac{\cos \theta_{bx} \cos \theta_{by}}{\sin \theta_p} - k_L D_{(k)} \right) \quad (13)$$

where $D_{(k)}$ = the drag force on sediment particle of size fraction k ; $W_{(k)}$ = the submerged weight of sediment particle of size fraction k ; $F_{(k)}$ = the friction force between the bed and sediment particle of size fraction k ; u_{bj} = component of near bed flow velocity in j direction; C_D = the drag coefficient; c_e = the coefficient accounting for the effective application area of the drag force; θ_{bx}, θ_{by} = the angle of the local bed inclination in x and y direction, respectively; θ_p = angle between \mathbf{p}_{b1} and \mathbf{p}_{b2} . When Eq. (10) is solved, the velocity components of a sediment particle are obtained. Hence, the position of a particle at any time after being picked up is known. After n th step of movement, the position of the particle belonging to size fraction k is as below.

$$\mathbf{p}_{sed(k,n)} = \mathbf{p}_{sed(k,n-1)} + \Delta t \cdot \mathbf{u}_{sed(k,n)} \quad (14)$$

where $\mathbf{p}_{sed(k,n)}$, $\mathbf{p}_{sed(k,n-1)}$ = the position of sediment particle after n th and $(n-1)$ th time step, respectively; Δt = time step; $\mathbf{u}_{sed(k,n)}$ = the sediment movement velocity. At this position, the total distant of movement of the particle from its original location is written as

$$s_{(k,n)} = \sum \Delta t |\mathbf{u}_{sed(k,n)}| \quad (15)$$

where $s_{(k,n)}$ = the movement distance of a sediment particle of size fraction k after n th time step.

c) Sediment deposition

During the transport stage, some of the sediment particles may keep moving following the trajectory as described above, while some of them may settle down and deposit onto the bed at certain place. The amount of sediment deposition onto the bed along the sediment transport trajectory is estimated with the aid of the probability density function for the step length, i.e.

$$V_{d(k,n)} = V_{p(k)} f_s(s_{(k,n)}) \Delta t |\mathbf{u}_{sed(k,n)}| \quad (16)$$

where $V_{d(k,n)}$ = the deposition volume of size fraction

k after n th step of movement; $f_s(s_{(k,n)})$ = the probability density function of step length and is estimated from the following expression.

$$f_s(s_{(k,n)}) = \frac{1}{\lambda_{(k)}} \exp\left(-\frac{s_{(k,n)}}{\lambda_{(k)}}\right) \quad (17)$$

where $\lambda_{(k)}$ = the average step length of sediment particle belonging to size fraction k , which is estimated following Einstein's suggestion as below (Einstein, 1950).

$$\lambda_{(k)} = \lambda_0 d_{(k)} \int_{-B_*/\tau, -1/\eta_0}^{B_*/\tau, -1/\eta_0} \frac{1}{\sqrt{2\pi}} \exp\left(-\frac{r^2}{2}\right) dr \quad (18)$$

where η_0 = coefficient of variation of lift force; $\lambda_0 = 100$ and $B_* = 0.156$, are two constants.

(3) Bed variation module

With the methods introduced above, the behavior of sediment particles is traced in an explicit way. Detailed information of sediment particles movement is obtained along their moving trajectories. In general, these trajectories do not coincide with the computational mesh. In order to simulate the bed deformation process, the information at the center of any computational mesh must be obtained based on that along the sediment moving trajectories. The change of the bed level is hence calculated in the following procedure: The pick-up volume of size fraction k from mesh i is calculated with Eq. (9). Then the position of sediment particles belonging to each size fraction after n th time step is estimated with Eq. (14). The corresponding deposition volume there is estimated from Eq. (16) and the mesh where the sediment particles locate is specified. The calculated deposition volume is then distributed to this mesh and its neighbors. For each mesh, the deposition amount is a summation of distributed deposition volume of sediment particles deposit within the mesh itself or its neighbors. As a result, the estimation of the change of the bed level becomes possible, i.e.

$$\frac{\partial z_b}{\partial t} = \frac{A_1 A_2}{A_3} \frac{\sum_k V_{d(k)} - \sum_k V_{p(k)}}{S_d} \quad (19)$$

where z_b = bed level; A_1 = shape coefficient of sediment particle for 1D geometrical properties (=1.0); $V_{d(k)}$ = the deposition volume of size fraction

k at mesh center; S_d = the projected area of the mesh onto the horizontal plane.

It has to be mentioned that after a group of sediment particles are picked up from a mesh, the movement of them is traced until all the particles deposit. Sometimes, it takes a long time for all the particles to settle down. In other words, new sediment particles are picked up from a mesh while the sediment particles picked up in the previous pickup event is still in motion. Since all the information should be memorized, it consumes exhaustive computer resources. For the time being, different time steps are used in this research for the computation of the pickup event and the deposition event. The time step for the pickup event is a little larger than that for the deposition event.

Besides the bed level, the bed composition also plays an important role in sediment transport modeling. In this study the bed sorting process suggested by Liu (1991) is adopted. The bed is vertically divided into an active layer, a transition layer and a series of deposition layers. The active layer changes its elevation and sediment size distribution with the transport of bedload but keeps a constant thickness. The change of the bed level is expressed by the changing of the thickness of the transition layer and the number of the deposition layers. Detailed information is referred to Liu (1991) and Zhang (2005).

(4) Solution procedure

The solution procedure of the numerical model is summarized as below.

- (a) Solve momentum equations for each velocity component.
- (b) The resulted velocity is used to calculate mass fluxes through CV surfaces. Improve velocity field in the SIMPLE method.
- (c) Solve transport equations for turbulence kinetic energy and its dissipation rate and update the eddy viscosity.
- (d) Repeat the above procedures until the residual level becomes sufficiently small.
- (e) Estimate the near bed flow velocity and shear stress.
- (f) Estimate sediment pickup volume at each time step. The volume is adapted to that for the time step used in the deposition calculation.

- (g) Compute sediment moving trajectory and deposition along the trajectory.
- (h) Estimate sediment deposition volume at each mesh.
- (i) Calculate bed level change at each mesh based on the pickup volume and deposition volume.
- (j) Calculate the change of bed composition.
- (k) Adjust local bed slope if it is larger than some critical angle (angle of repose underwater is used in this research for simplicity). Corresponding adjustment in the bed composition is made as well.
- (l) Generate new mesh for next computation.

3.2 Computational conditions

The numerical model is used to simulate the flow field and bed variation process in the experimental flume. Two of the experimental cases are selected in the numerical simulations: Case2 and Case8. The movable bed consists of uniform sediment in Case2 and it is non-uniform in Case8. However, it may be noted that the mean size of the sediment used in these two cases is very close.

Unstructured mesh is used in the simulations in order to test the performance of the model. The plan view of the computational mesh in the neighborhood of the spur dyke is shown in Fig.3. The mesh is hybrid consisting of both hexahedra and prisms. The total mesh number is 6344 and the total node number is 4030.

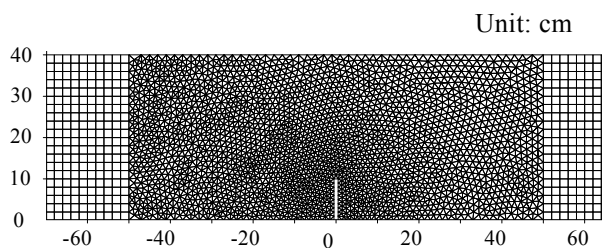
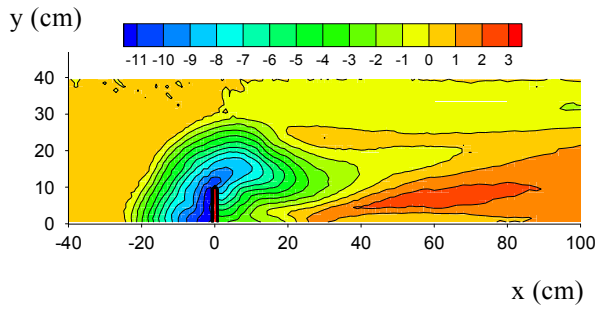
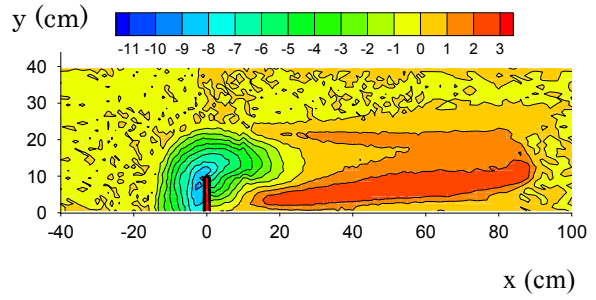


Fig.3 Plan view of the computational mesh

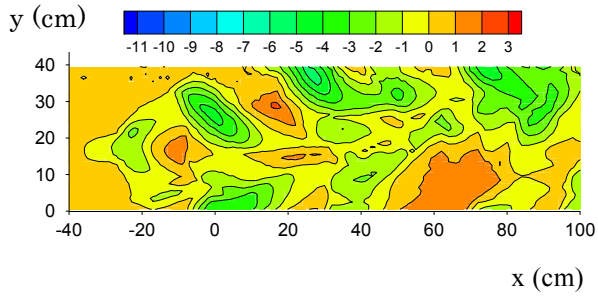
The computational domain is not the same as the experimental domain. It covers a 2.4m-long reach of the experimental flume longitudinally with the spur dyke at the middle of the reach in order to save computational time. Simulations are finished after a 2-hour bed deformation process since the movable bed shows insignificant changes and a quasi-equilibrium stage is reached.



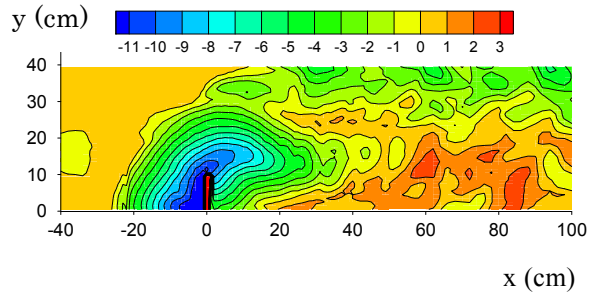
(a) Case 2



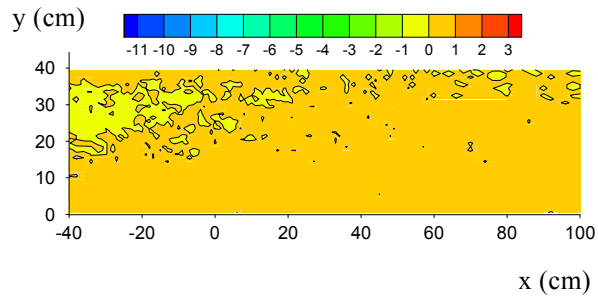
(b) Case 4



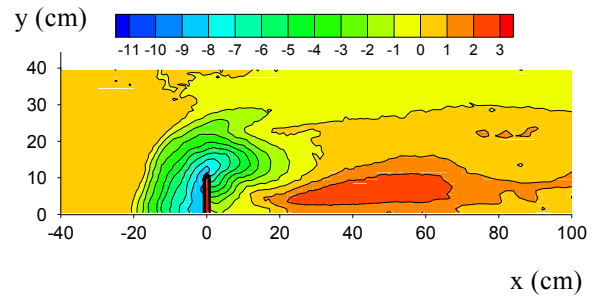
(c) Case 5



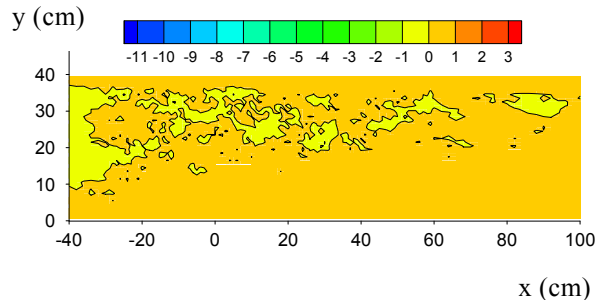
(d) Case 6



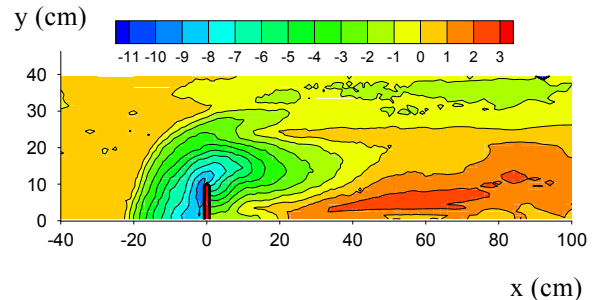
(e) Case 7



(f) Case 8



(g) Case 9



(h) Case 10

Fig.4 Final bed configuration (Experiment results)

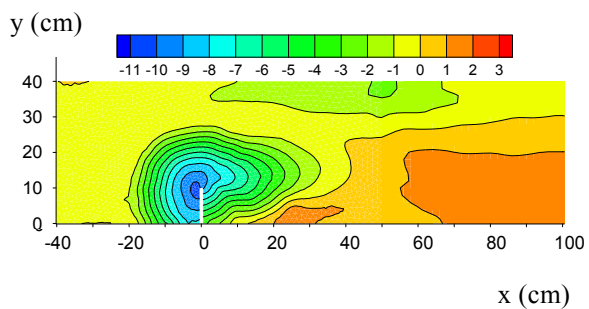


Fig.5 Simulated bed configuration (Case2)

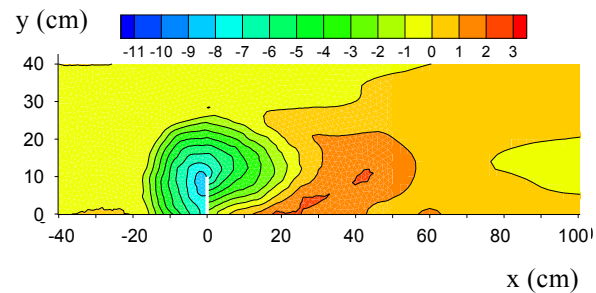


Fig.6 Simulated bed configuration (Case8)

4 Results and Discussions

4.1 Bed configuration

The bed contours at the final stage in the experiments are shown in Fig.4. The contours of cases without any spur dyke are firstly discussed, which provide reference information for the investigation on the impacts of the spur dyke later. For uniform sediment bed in Case5, bed forms develop as the critical shear stress is smaller than the actual bed shear stress. For non-uniform sediment beds in Case7 and Case9, bed shear stresses are smaller than the critical ones calculated based on sediment mean diameters. But bed change is still observed although the magnitude is very small. This is a typical phenomenon taking place in alluvial rivers and the reason has been well documented. Due to the selective transport of fine particles, bed will be degraded. On the other hand, the remaining particles in the surface layer become shelters for the particles beneath them and prevent the bed from further degradation. It has to be mentioned that a few amount of coarse particles are captured by the sediment trap at the downstream of the flume in the experiment. The change of inter-particle contact conditions after the erosion of fine particles is considered to be mainly responsible for this phenomenon.

The contours in Fig.4 demonstrate that the presence of the spur dyke has significant impacts on the bed configuration. In the approach flow area, one may find that the bed level shows insignificant change, indicating a reduction of shear stress there. The main features of the deformed bed are a local scour hole, followed by a long distance of deposition area. These features can be evidently observed in the contours shown in Fig.4. In order to clarify the change of the bed configuration around the spur dyke, in particular the local scour dimensions, a summary is presented in Fig.7 including the main features of the surface extent of the scour hole. The values of the key parameters resulting from the current experiments are shown in Tab.3.

For relatively uniform sediment bed (i.e. Case2, Case4 and Case6), the maximum scour depth and the area of the scour extent increase with the decreasing of the sediment mean diameter, which is

easily observed from the contours in Fig.4. The quantitative evidence is shown in Tab.3 with the values of a/L , b/L , c/L and d_{max} . It may be explained that the entrainment of coarse particles necessitates more flow energy and hence they are not easily eroded. The representative slopes of the scour hole also show some relation with the mean sediment diameter. Take a look at θ_1 , θ_2 and θ_3 in Tab.3, one may conclude that the slope of the scour hole is relatively steeper in case of coarser sediment. Moreover, compared with the slope upstream and in front of the spur dyke, the slope is very gentle at the downstream part of the scour. It is the result of the adjustment with the local flow field, especially the vortex system. Case6 deserves special attention since it is conducted under live-bed scour condition and without sediment supply from the upstream boundary. Besides the local scour area, erosion also appears in the downstream of the spur dyke due to the development of bed forms. Compared with Case5, the bed forms in Case6 are superimposed upon the bed configuration caused by the spur dyke, having sophisticated features and dimensions.

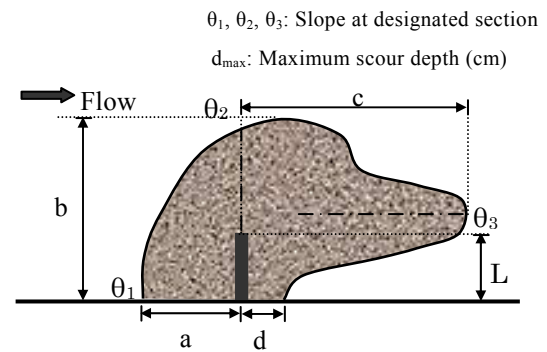


Fig. 7 Sketch of scour dimensions

Table 3 Scour dimensions

	Case2	Case4	Case6	Case8	Case10
a/L	2.1	1.4	2.4	1.9	2.1
b/L	2.9	2.3	4.0	2.9	3.0
c/L	4.0	2.1	3.9	2.3	3.7
d/L	1.4	0.0	1.4	0.4	0.9
θ_1	26°	34°	26°	27°	22°
θ_2	31°	33°	29°	26°	25°
θ_3	16°	18°	14°	19°	12°
$d_{max}(cm)$	11.4	9.1	12.1	9.2	9.4
$d(mm)$	1.03	1.70	0.31	1.00	0.86

Should one take a look at the cases of non-uniform sediment only (i.e. Case8 and Case10), similar

conclusion would be drawn that the increasing of the mean sediment diameter will result in decreasing of the local scour depth and the scour extent area as well as increasing of local bed slopes of the scour hole. It has been mentioned that the movable bed in Case8 is gap-graded and that in Case10 is well graded. But this difference seems not affect so much on the scour geometry under the current experimental conditions. However, the non-uniform sediment beds do show different features from those of the uniform ones if one compares all the listed cases. It is very clear that the maximum scour depth in either Case8 or Case10 is much smaller than that in Case4, although the mean sediment diameter in the former case is slightly smaller than the latter one. It seems to be summarized that the local scour will be smaller in a non-uniform sediment bed compared with a uniform one with the same mean diameter. The formation of an armor layer at the bottom of the scour hole is a probable reason. The local slopes of the scour hole seem to be milder in a non-uniform sediment bed if only θ_1 and θ_2 are taken into account. Further experiments are needed to validate it.

The numerical results for Case2 and Case8 are plotted in Fig.5 and Fig.6. The maximum local scour depths are 10.4cm and 8.6cm after 2hours, respectively. Compared with those of the experimental results (11.4cm and 9.2cm after 3hours, respectively), the predicted results are quite well. The geometries of the scour holes are also similar to those of the experiments but exhibit slight differences. The reason is not evidently clarified. However, similar phenomena have been observed by Zhang and Nakagawa (2008b) in similar simulations with sediment transport models of equilibrium type. It might imply that the problem is caused by the inherent deficient of the turbulence model or improper interpretation of the information from the turbulent flow domain to the near bed flow domain.

4.2 Bed composition

The non-uniformity of sediment particles affects not only the bed configuration but also the bed composition, in particular in the bed surface. The changes of the bed composition in Case8 are plotted in Fig.8 and Fig.9. Fig.8 is a sampling result from the experiment while Fig.9 shows the prediction with the numerical model. In both figures, the bed

surface is coarsened in most of the area and there are two belts consisting of relatively fine sediment. One belt is near the side of the flume and starts from the spur dyke wake, while the other one is near the longitudinal centerline of the flume and starts from the head of the spur dyke. The two belts are not readily distinguished from the bed contours shown in Fig.4 and Fig.6.

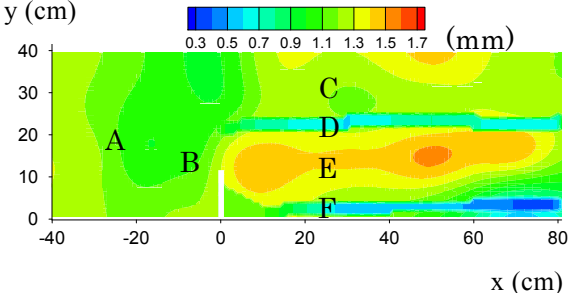


Fig.8 Mean size distribution (Case8, Experiment)

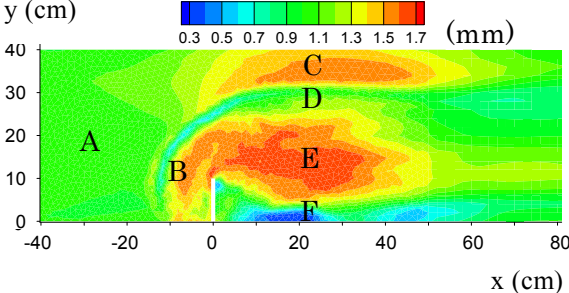


Fig.9 Mean size distribution (Case8, Simulation)

For clarity, the area around the spur dyke is divided into 6 zones as shown in Fig.8 and Fig.9. Zone A stands for the approach flow area and Zone B is the local scour hole. Zone C and Zone E represent the places where sediment is obviously coarsened. Zone D and Zone F are the belts with relatively fine sediment. It is very obvious that the numerical result is quite encouraging if one compares the results in all those zones. In particular, the capability to predict the alternate distribution of fine and coarse sediment particles demonstrates that the numerical model is powerful. On the other hand, attention should also be paid to the differences between the experimental and computational results. In Zone B, one may find that the lower part of the scour hole is relatively coarse while the upper part of which is rather fine. It is due to the existence of a vortex system in the scour hole. There are some differences between the experimental and numerical

results. The omission of the suspended load in the numerical model might be responsible for these differences. Due to strong vortices in the scour area, some of the sediment particles transport as suspended load in the scour hole. These particles move to the downstream as bedload in the computation as they are not coarse enough. Consequently, the bottom of the scour hole becomes very coarse. However, they are suspended in the scour area in the experiments and settle down when the pump is stopped. In Zone C and Zone E, the mean sizes of sediment particles are also overestimated in the simulation. This discrepancy might be resulted from the discrepancy in the prediction of the local bed configuration and hence, the local flow field. Moreover, Zone D in the experiment is slightly closer to the longitudinal centerline of the flume than that in the simulation. The discrepancy in the prediction of the bed configuration as well as the corresponding local flow field is also believed to be the cause. Nevertheless, further investigations with more computational cases are needed.

The alternate distribution of fine and coarse sediment is also observed in another experiment case, i.e. Case10, which demonstrates the generality of this phenomenon for non-uniform sediment beds. It is known that the change of the size distribution of sediment particles in the bed surface is closely related to the complex flow structure in the proximity of the spur dyke. Under the complex flow condition, sediment particles of different sizes take their moves following different trajectories. The detailed flow structure around a spur dyke is not shown here, which may be found in many references such as Zhang et al. (2009). Instead, a sketch of the movement of sediment particles near the bed in Case8 is shown in Fig.10 according to experimental observations.

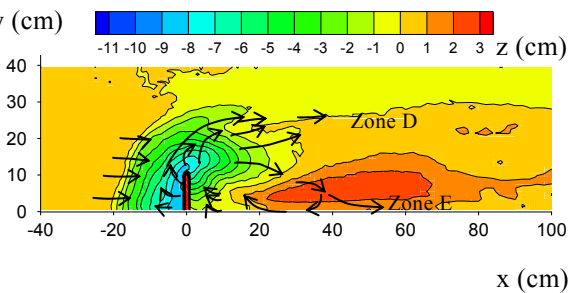


Fig.10 Sketch of sediment movement

Due to the difference in sizes, the entrainment conditions, movement trajectories and the travelling time vary a lot for different sediment particles even under the same flow conditions. As a result, the size distribution patterns shown in Fig.8 and Fig.9 are formed.

5 Conclusions

In this paper, a recent study was presented on the non-uniform sediment transport around a spur dyke with both experimental and numerical methods.

Experimental data indicates that a spur dyke has significant impacts on the bed configuration and bed composition. For relatively uniform sediment bed, the maximum scour depth and the scour area increase with the decreasing of the particle diameter. While the local slope of the scour hole increases with the increasing of the particle size. The local scour in a non-uniform sediment bed is generally smaller compared with that in a uniform bed of the same sediment mean diameter. In the local scour hole, the bottom part is rather coarser than the upper part. Due to the sediment sorting process, the bed materials generally become coarser in the neighborhood of the spur dyke and armor layers form there. However there exist two longitudinal belts consisting of relatively fine sediment.

The numerical model is based on unstructured mesh, being able to solve problems in complex geometries and/or with irregular boundaries. The model takes into account the stochastic and deterministic nature of sediment transport, capable of simulating sediment transport in non-equilibrium conditions. The simulated local scour and size distribution around the spur dyke are in reasonable agreement with those of the experiments. However, the model still needs refinement to improve the accuracy of flow velocity prediction and to shorten the computation time. Moreover, fundamental experiments are also needed to investigate the underlying processes associated with the pickup and deposition events of non-uniform sediment particles.

Acknowledgements

This research is supported in part by a research grant from the Kinki Construction Association,

Japan (PI: H. Zhang, No.25-1) and the GCOE-HSE Program (Kyoto University Global Center for Education and Research on Human Security Engineering in Asian Megacities, PI: Y. Matsuoka).

References

- Einstein, H. A. (1950): The bed-load function for sediment transportation in open channel flows, Technical Bulletin, No. 1026, U.S. Department of Agriculture, Soil Conservation Service, Washington D.C.
- Liu, B.Y. (1991): Study on Sediment Transport and Bed Evolution in Compound Channels, Ph.D Thesis, Kyoto University.
- Nagata, N., Hosoda, T., Nakato, T. and Muramoto, Y. (2005): Three-dimensional numerical model for flow and bed deformation around river hydraulic structures, *Journal of Hydraulic Engineering*, ASCE, Vol.131, No.12, pp. 1074-1087.
- Nakagawa, H., Tsujimoto, T. and Murakami, S. (1986): Non-equilibrium bed load transport along side slope of an alluvial stream, *Proceedings of the 3rd International Symposium on River Sedimentation*, University of Mississippi, pp. 885-893.
- Onda, S., Hosoda, T., Kimura, I. and Iwata, M. (2007): Numerical simulation on local scouring around a spur dyke using equilibrium and non-equilibrium sediment transport models, *Annual Journal of Hydraulic Engineering, JSCE*, vol.51, pp.943-948 (in Japanese).
- Zhang, H. (2005): Study on Flow and Bed Evolution in Channels with Spur Dykes, Doctoral Dissertation, Kyoto University.
- Zhang, H. and Nakagawa, H. (2008a): Scour around spur dyke: recent advances and future researches, *Annals of the Disaster Prevention Research Institute, Kyoto University*, No. 51B, pp. 633-652.
- Zhang, H. and Nakagawa, H. (2008b): Investigation on morphological consequences of spur dyke with experimental and numerical methods, *Advances in Hydro-science and Engineering* (Wang, Kawahara, Holtz, Tsujimoto & Toda eds), Vol.8, Nagoya, Japan, CD-ROM.
- Zhang, H., Nakagawa, H., Kawaike, K. and Baba, Y. (2009): Experiment and simulation of turbulent flow in local scour around spur dyke, *International Journal of Sediment Research*, Vol.24, No.1, pp. 33-45.